

Effect of Co doped material on the structural, optical and magnetic properties of Cu_2O thin films by SILAR technique

K. Dhanabalan^{1,2} · A. T. Ravichandran² · K. Ravichandran³ · S. Valanarasu⁴ · Srinivas Mantha⁵

Received: 7 July 2016 / Accepted: 11 November 2016 / Published online: 22 November 2016
© Springer Science+Business Media New York 2016

Abstract Undoped and Co doped Cu_2O ($\text{Cu}_{2-x}\text{Co}_x\text{O}$; $x = 0, 1, 2, 5$ and 10) thin films were deposited onto glass substrates using successive ionic layer adsorption and reaction technique. The variation in the concentration of Co shows significant impact on the film properties, where as doped with 10 wt% of Co exhibited major property improvements when compared with other films. The prepared films were characterized for their structural, morphological, optical and magnetic properties. X-ray diffraction analysis of the films revealed the crystalline growth of $\text{Cu}_{2-x}\text{Co}_x\text{O}$ films. The substitution of Cu^{2+} by Co^{2+} ions has led to a single phase cubic structure highly oriented along (111) plane. Optical studies (photoluminescence and UV–vis–NIR) of the films exhibit the quality of the films with the increase of dopant. The stretching vibrations of Cu–O and O–Cu–O have been confirmed by Fourier transform infrared spectroscopy. The morphological study done by a field emission scanning electron microscope has shown as increase of particle size with

increase in the dopant concentration. High resolution of transition electron microscope and particle analyzer verified the nano-size and shape of the films. The presence of copper in the structure of thin film was confirmed by energy dispersive X-ray spectrometer. Magnetic measurements showed that undoped and minimum doped (1 and 2 wt%) films exhibit diamagnetic behavior and at the maximum (10 wt%) Co doping level, the films exhibit ferromagnetic properties. Current verses voltage studies showed the ohmic nature of the films.

1 Introduction

Metal oxide materials have received great attention for their physical and chemical properties. Copper oxide thin film is a p-type semiconducting metal oxide material and it exhibits direct band-gap (~ 1.3 to 2.1 eV) [1]. Copper oxide exists, in two forms of cupric oxide (or) copper monoxide (CuO) and Cuprous oxide (Cu_2O) [2]. Cu_2O materials are especially useful in the field of Photovoltaic devices and light emitting diodes [3]. Because of the copper ore (Cu_2O), the active layer is widely available as naturally occurring minerals. Cu_2O is the parent compound of many p-type transparent conducting oxides (TCOs) such as Cu_xO_2 delafossites ($X = \text{Co}, \text{Fe}, \text{Zn}, \text{Al}, \text{KCL}, \text{Cr}, \text{etc.}$) [4]. The magnetic property of the Cu_2O material can be enhanced with doping of Co and Fe without affecting the semiconductivity. Generally, metal doping materials are making radical changes in electrical, optical, morphologies and magnetic properties of copper oxide thin films [5]. Over the past decade, 1D and 2D nanostructures have been discussed for their unique optical, electrical and mechanical properties [6]. In recent years, tremendous effort has been dedicated to converting 1D and 2D nanostructures

✉ A. T. Ravichandran
atrnc@gmail.com

¹ Department of Physics, J. J. College of Arts and Science (Autonomous), Pudukkottai, Tamil Nadu 622 422, India

² Post Graduate and Research Department of Physics, National College (Autonomous), Tiruchirappalli, Tamil Nadu 620 001, India

³ Post Graduate and Research Department of Physics, AVVM Sri Pushpam College (Autonomous), Poondi, Thanjavur 613 503, India

⁴ Post Graduate and Research Department of Physics, Arul Anandar College, Karumathur, Madurai, Tamil Nadu 625 514, India

⁵ IEEE Communications Society, Hyderabad 500 055, India

into 3D nanostructures [7]. Cu_2O is a suitable candidate for Bose–Einstein condensation because the binding energy is high. The material can be used in a wide range of applications such as gas sensors [8], Solar energy [9, 10], lithium ion batteries [11], photo catalyst [12–18], dilute magnetic semiconducting materials [19], transparent conductors [20] and water splitting under visible light irradiation [21–29]. Several methods can be employed in the deposition of Cu_2O thin film techniques, such as chemical vapour deposition [30], electro deposition [31], thermal oxidation [32], hydrothermal deposition [33], reactive sputtering [34, 35], one step hydrothermal [36] and chemical bath deposition (CBD) [37]. The preparation technique to be chosen varies depending upon the applications. The SILAR technique is also known as solution based atomic layer deposition (SALD) or the modified chemical bath deposition (M-CBD) technique [38–40]. It is very useful to prepare nanostructure thin non-toxic films at low cost and low temperatures. This method was good control over the deposition process, reaction condition and feasibility for large area deposition. All the films are investigated for their structural, optical, electrical, and morphological properties based on the deposition time.

2 Experimental procedure

Substrate cleaning is one of the important factors in the deposition of thin films. Glass slides of $26 \text{ mm} \times 76 \text{ mm} \times 1 \text{ mm}$ dimensions were used as substrates. These substrates were boiled in concentrated chromic acid for 2 h, then cleaned with double distilled water and finally rinsed with acetone before the deposition of the films. Many trials were carried out for optimizing the good quality of copper oxide thin films for undoped and Co doped Cu_2O (1, 2, 5 and 10 wt%) thin films onto glass substrates using SILAR technique. The high purity chemicals (>99%) such as copper sulphate pentahydrate ($\text{CuSO}_4 \cdot 5\text{H}_2\text{O}$), sodium thiosulfate ($\text{Na}_2\text{S}_2\text{O}_3 \cdot 5\text{H}_2\text{O}$), Cobalt sulphate (CoSO_4), and sodium hydroxide (NaOH) were used as precursor solutions without further purifications. Initially, 1 M NaOH solution was prepared with deionized water and maintained at 80°C through out the experiment. Then, the precursor solutions of ($\text{CuSO}_4 \cdot 5\text{H}_2\text{O}$) and ($\text{Na}_2\text{S}_2\text{O}_3 \cdot 5\text{H}_2\text{O}$) were prepared and the required concentration of 0.1 M was constantly stirred. Then 1, 2, 5 and 10 wt% of CoSO_4 were added to the precursors and mixed systematically using a magnetic stirrer. The deposition cycle of the thin film formations consists of three steps. (1) The cleaned glass substrate was immersed in hot NaOH (80°C) solution for 20 s. (2) Instantly, the substrates were immersed in copper thiosulphate complex solution for 20 s. (3) Rinsing the substrate with ample amount of deionized water bath for 10 s to remove the unreacted Cu^+

and OH^- ions loosely bounded particles from the substrate. A schematic representation of the SILAR method is shown in Fig. 1. The process was repeated up to 30 cycles, to obtain good quality of undoped and Co-doped Cu_2O thin films. The deposited films were characterized extensively using the following instruments. X-ray diffraction pattern of the films was obtained using X'pert PRO (PANalytical) diffractometer with $\text{CuK}\alpha$ radiation ($k = 0.15405 \text{ nm}$) in steps of 0.1 over the 2θ range of 15° – 75° . Morphological examination of the films was done using Hitachi (S-3000H) scanning electron microscope. HRTEM images and electron diffraction patterns for the film layers were measured using the JEOL JEM 2100, 200 kV operating voltage. In order to determine the band gap energy of the films, the optical transmission was recorded using Perkin Elmer Lambda 35 spectrophotometer. Current versus voltage are analyzed using Keithley sourcemeter 2450. The results are discussed below.

3 Results and discussion

3.1 Structural studies

The X-ray diffraction patterns of the undoped and Co-doped Cu_2O thin films are shown in Fig. 2. In the case of undoped film, the diffraction line corresponds to (111) plane and a weak peak correspond to (200) planes of Cu_2O (JCPDS card No. 05-0667). When cobalt is doped with the Cu_2O , the intensity of the (111) plane increases suddenly to a high value (nearly four times) and the intensity decreases with further increase in Co-doping level. The low intensity of the diffraction line in the case of the undoped film may be ascribed to the presence of a large number of Cu and O vacancies in the Cu_2O lattice. But, when Co is doped with the Cu_2O , the Cu^{2+} and O^{2-} ions may be settled at the Cu

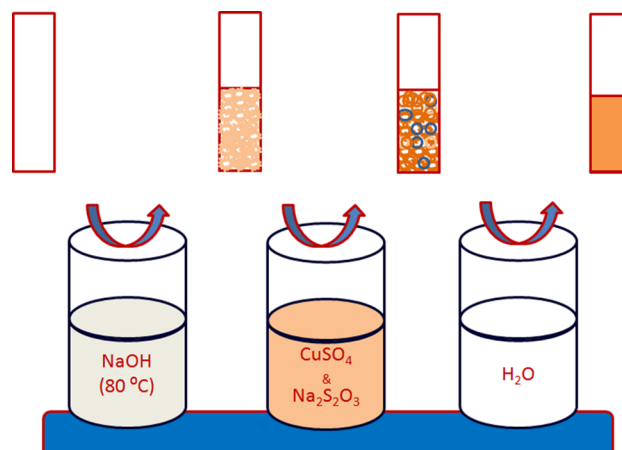


Fig. 1 A schematic representation of the SILAR method

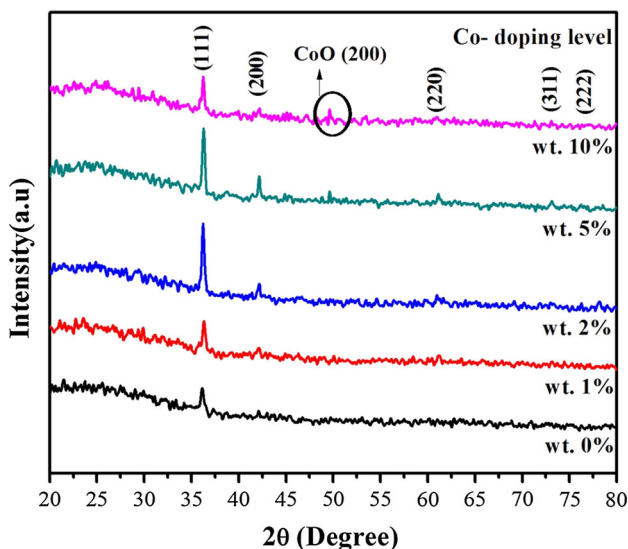


Fig. 2 XRD patterns of undoped and Co-doped Cu₂O thin films

and O²⁻ vacancies, respectively, improving the periodic alignment of ions in the lattice. When the doping level is increased, the excess Co ions take the interstitial positions, degrading the crystalline quality, resulting in a decrease in the intensity of X-ray diffraction lines. A close observation of the XRD patterns revealed that at the highest examined doping level (10 wt%) there was a diffraction peak at the 2θ value of 49.62° associated with the (200) plane of CoO (JCPDS data card No: 09-0402) indicating the presence of a secondary phase (Fig. 2).

The observed shift in the position of the prominent peaks towards the higher angles when the Co doping level is increased is an evidence for the interstitial of Co ions into the Cu sites. It is a well-known fact that the right shift indicates the narrowing of the ‘d’ spacing. Here, as the ionic radius of Co²⁺ (72 pm) is less than that of Cu⁺ (77 pm), this reduction in the ‘d’ spacing is an expected result. The crystallite size of the film was calculated using Debye–Scherrer’s formula [41–44]

$$D = \frac{0.9\lambda}{\beta \cos \theta} \tag{1}$$

where D—is the crystallite size, K—is the shape factor (K = 0.9), λ—is the wave length of X-rays, β—is the full-

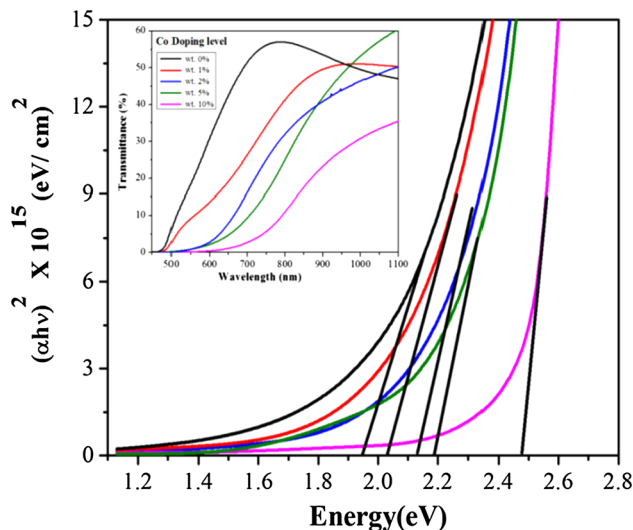


Fig. 3 Tauc’s plots for the undoped and Co-doped Cu₂O thin film

width at half maximum (FWHM). The lattice parameter ‘a’ of the cubic system of Cu₂O film and dislocation density are calculated using the formulae [45] and the values are given in Table 1.

$$\frac{1}{d^2} = \frac{h^2 + k^2 + l^2}{a^2} \tag{2}$$

$$\delta = \frac{1}{D^2} \tag{3}$$

3.2 Optical properties

Optical transmittance spectra of the undoped and Co-doped film with different wt% were recorded in the range of 450–1100 nm are shown in Fig. 3-inset. The energy band gap of the material can be determined by the decreases in transmittance. The transmittance of the film is obtained for nearly UV region as well as for the undoped and Co-doped material. The transmittance of the undoped film is higher than that of the doped film (Co—1, 2 and 5 wt%) gradually decreases with increases of the Co-doped material. The high transmittance of the material in the visible region is used for aesthetic window glass materials. The fundamental absorption can be used to determine the band gap of

Table 1 Structural and optical parameters of undoped and Co-doped Cu₂O thin films

Doping concentration	Crystallite size (D) nm	Dislocation density (δ) (lines/m ²)	a* (Å)	Energy band gap (eV)
Co 0%	62.83	2.53	2.48544	1.94
Co 1%	53.30	3.52	2.47828	2.03
Co 2%	48.47	4.26	2.47440	2.12
Co 5%	39.24	6.49	2.47866	2.18
Co 10%	28.44	12.36	2.47683	2.47

* Standard data: a = 2.4650 Å (JCPDS Card No: 05-0667)

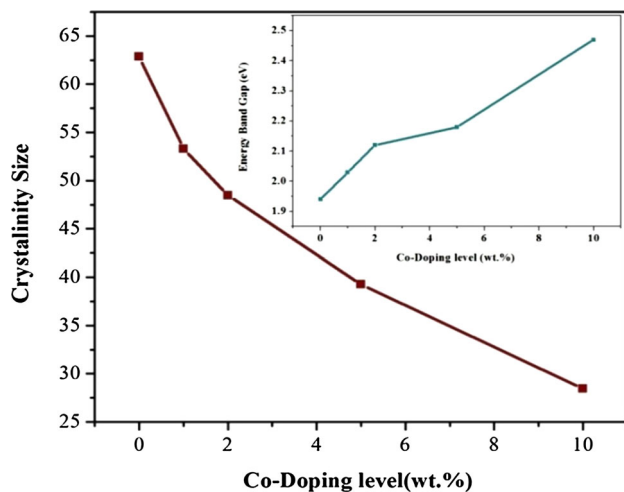


Fig. 4 The plot for calculated band gap for the undoped and Co-doped Cu_2O thin films and optical transmittance (*inset*)

the film. Figure. 3 shows the band gap of the films as estimated from the Tauc's plot relation [46–50] of absorption co-efficient (α) and the photon energy ($h\nu$) as

$$(\alpha h\nu)^2 = A(h\nu - E_g) \quad (4)$$

where A and E_g are the constant and optical band gaps, respectively. The E_g can be determined by extrapolation of the linear portion of the curve to the $h\nu$ axis. The band gap of the film increases with increases in doping level, carrier concentration, and the decreased crystallite size (D). Figure. 4 shows the variation of crystallite size and Energy band gap with undoped and Co doped films.

3.3 FTIR studies

The Fourier transform infrared (FTIR) spectrum is investigated and it confirms the formation of copper oxide of the material. Figure 5 shows the FTIR spectra (range 480–4000 cm^{-1}) of the copper oxide thin films (undoped and Co-doped (1, 2, 5, 10 wt%)). In all the films, the peaks

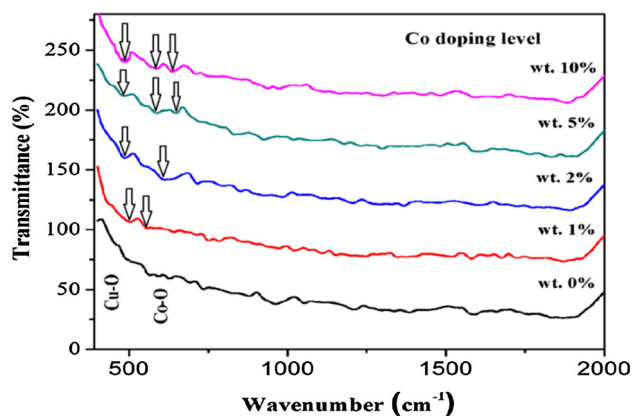


Fig. 5 FTIR spectra of undoped and Co-doped Cu_2O thin films

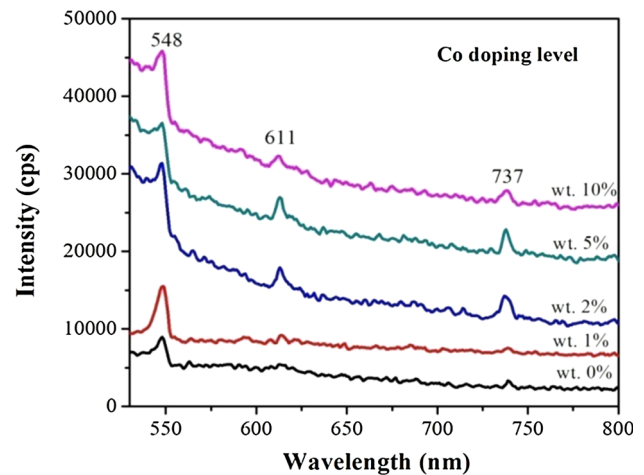


Fig. 6 Photoluminescence (PL) spectra of undoped and Co-doped Cu_2O thin films

at 425 and 574 cm^{-1} are corresponding to the stretching vibrations of Cu–O [51]. The peak at 618 cm^{-1} is attributed to the formation of Cu_2O [52]. The broad band absorptions between 1300 and 2000 cm^{-1} reveal the presence of H_2O and CO_2 molecules. The peaks in the region 700–900 cm^{-1} are ascribed to the formation of Co–O stretching vibrations [53]. The peaks at 1583 and 3559 cm^{-1} are assigned to C–O and O–H, respectively.

3.4 Photoluminescence (PL) studies

Figure. 6 shows the room temperature photoluminescence (PL) spectra of undoped and Co-doped Cu_2O films. The PL spectra reveal the electron–hole separation and recombination. The films exhibit PL peaks at wavelengths 548, 611 and 737 nm. In all the films, the NBE peaks are appeared at 548 nm [54]. It is found to be shifted towards the lower wavelength (blue shift) as the Co-doping levels increased up to 10 wt%. The defect level peak observed at the wavelength 611 nm. The defect level peak centered at 737 nm may be related to the relaxed excitons at Cu or O vacancies as shown in Fig. 6. It is attributed to the Moss–Burstein effect. It can be attributed to the variation of the optical band gap of the material.

3.5 Surface morphological with EDAX, EDX mapping and TEM studies

Figure. 7 shows the scanning electron microscope images of undoped and Co-doped Cu_2O thin films on glass substrate. In the undoped films one can see a large number of small particles agglomerated, due to Van-der Waals force [55] they combine to form large grains with different sizes of nanometry. The image of 1% Co doped, particles is loosed from the grain, because the doping of Co induces a

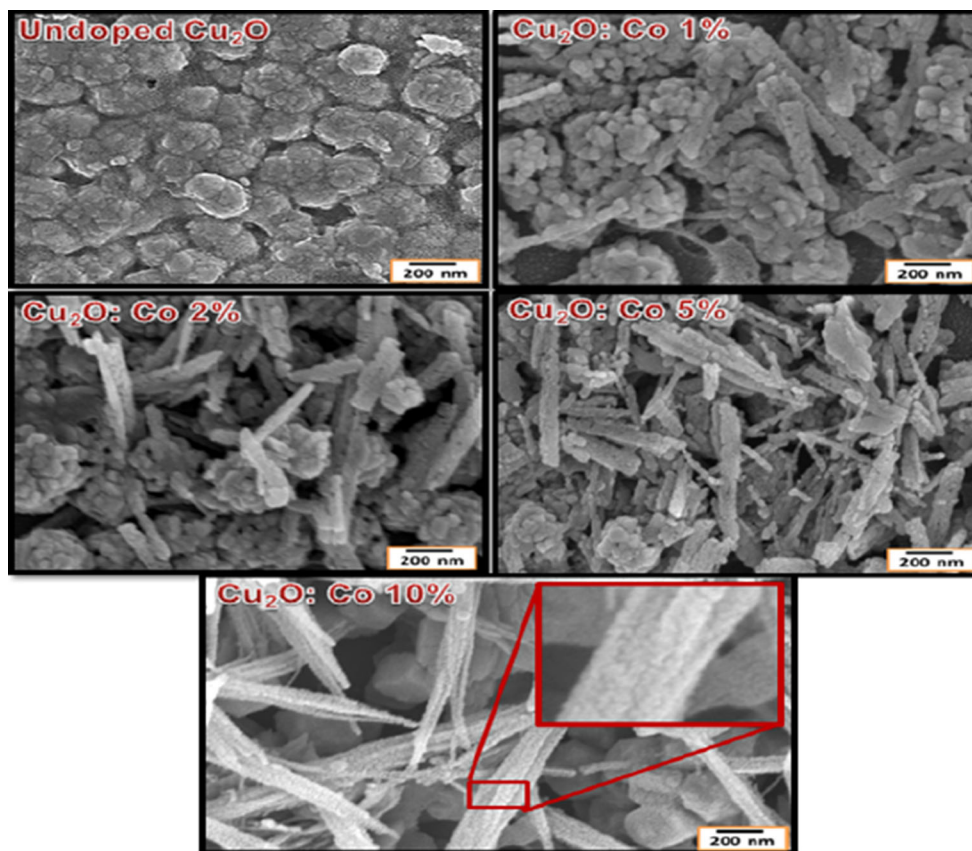


Fig. 7 FESEM images of undoped and Co-doped Cu_2O thin films

dilution of the binding energy of the host material. Simultaneously the loosed particles realign to form rod-like structures with different length and breadth. A large number of rod-like structures appear with increasing doping levels of 2 and 5 wt%, with higher doping levels of one sees a decreasing in the grain size and the grains align together to form a combined needle-shape structure on the primary surface. The cubic structure of the grains is visible on the surface. This is strong evidence of the CoO in the cubic system of Cu_2O . This result corresponds with the structure analysis obtained for the X-ray diffraction. The EDAX spectrum of the Co (10 wt%) doped Cu_2O films is shown in Fig. 8. The spectrum (image) confirm the presence of the anticipated elements like Cu, O and Co.

The elemental compositions of the cobalt doped film were studied by energy dispersive X-ray mapping and the results are displayed in Fig. 9. The figure shows the presence of O, Cu and Co. The element maps demonstrated that O, Cu and Co are homogeneously distributed on the surface of samples.

The Fig. 10a–e shows the TEM, HR-TEM and SEAD images of undoped and Co-doped Cu_2O thin films for 1, 2, 5 and 10% respectively. The TEM images are found to be consistent with the SEM results. The HR-TEM images

clearly depict the uniform growth of the film along (111) plane as the lattice fringes are found to be regularly arranged with the interplaner spacing of 0.246 nm. The magnification of HR-TEM are insets in the top right corner of TEM images. It is well known that the ‘d’ spacing corresponding to the (111) plane of cubic structure of Cu_2O is 0.245 nm (JCPDS Card No: 05-0667). The SEAD pattern of TEM image (Co-doped with 10% of Cu_2O film) are presented in Fig. 10f. The pattern well matches with the cubic structure of the Cu_2O . This result is in good agreement with the XRD observation.

3.6 Vibrating sample magnetometer (VSM)

Magnetization measurements were carried out by using a vibration sample magnetometer (VSM) at room temperature. The studies can be clearly observed from the magnified parts of the M–H curves, indicating the diamagnetic order in $\text{Cu}_{2-x}\text{Co}_x\text{O}$ ($x = 0, 1, 2, 5, 10$ wt%). When the iron material of Co-doped, the magnetization properties changes from diamagnetic (high magnetization) to paramagnetic (low magnetization) behavior with changing concentrations of doping level. Undoped Cu_2O has a diamagnetic property [56]. This result agrees with the Fig. 11

Fig. 8 EDAX spectrum of Co doped Cu₂O thin film with 10 wt%

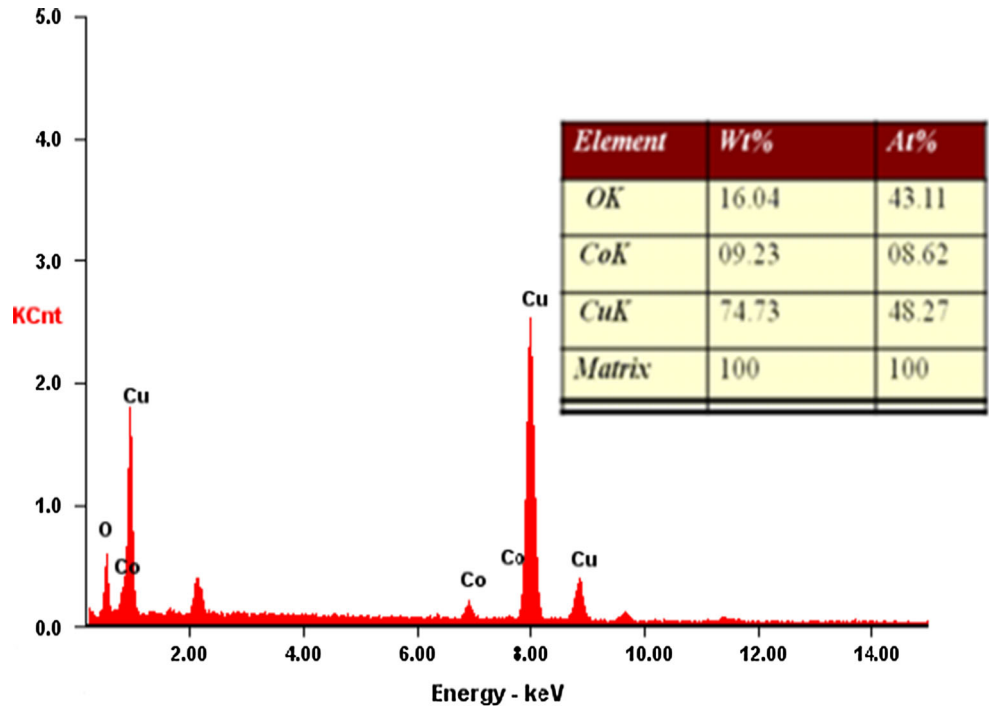
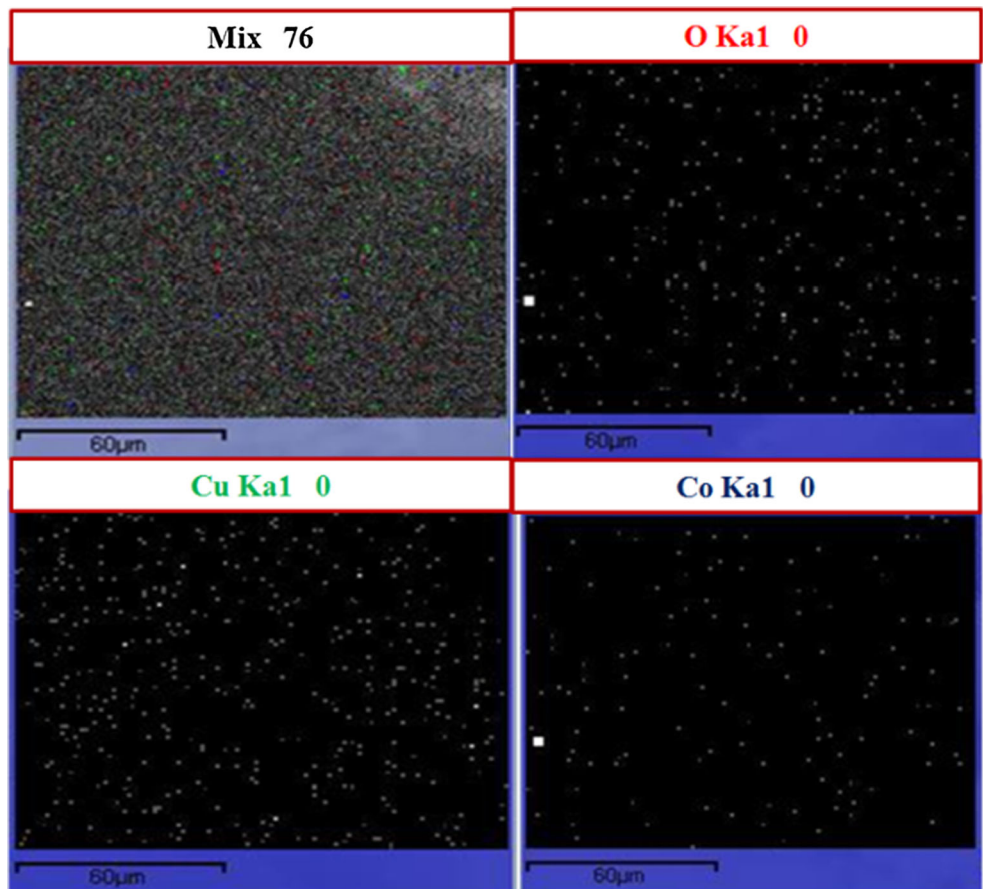


Fig. 9 Elemental EDX mapping of O, Cu and Co obtained from Co doped Cu₂O films



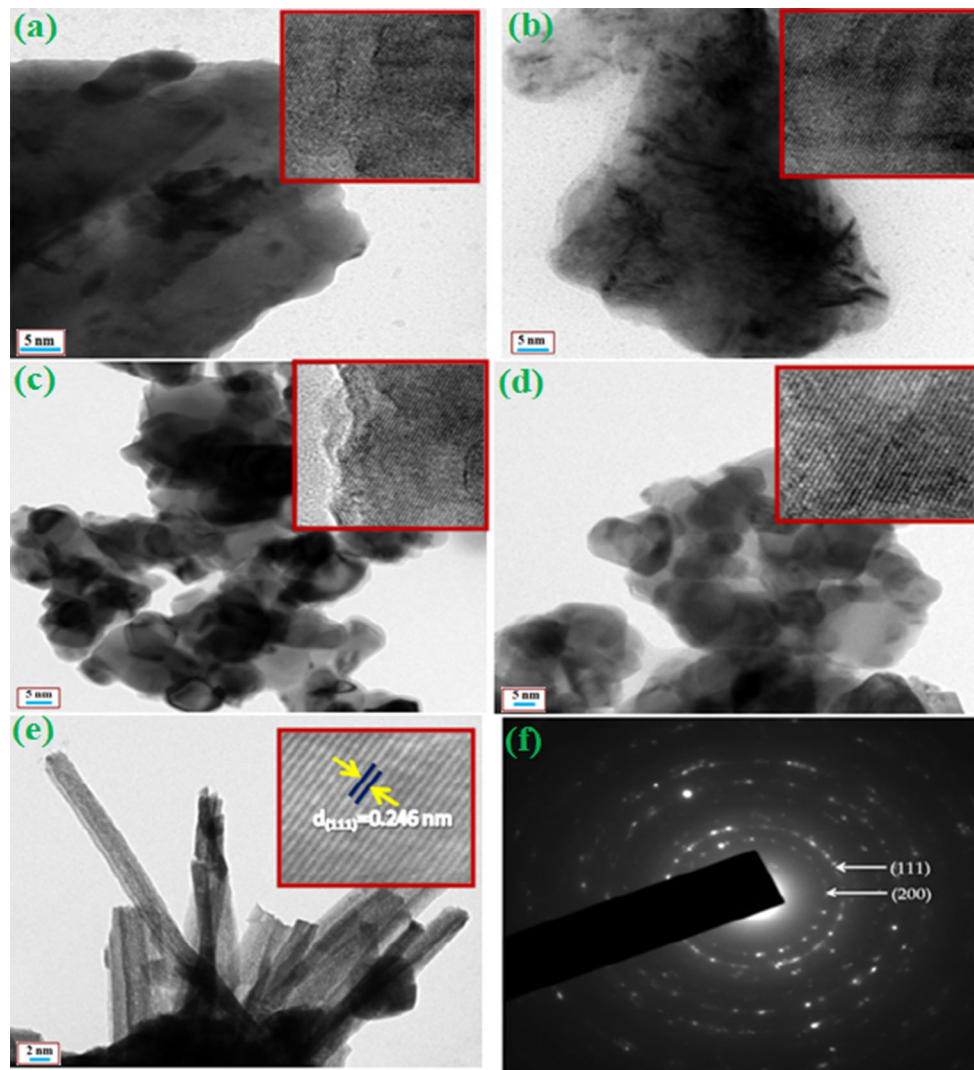


Fig. 10 TEM and HRTEM images of undoped and Co-doped films (Fig. 10 f SEAD pattern of 10% Co-doped Cu_2O film)

that shows the variation of magnetization against the applied magnetic field ($M-H$). The doping level of 1, 2 and 5 wt% exhibit and maintain the diamagnetic property. When the doping level reaches as 10 wt% the diamagnetic properties disappear and of paramagnetic properties [57]. The ferromagnetic (low magnetization) behavior is perhaps due to the intrinsic coupling (Co–Co) between the atoms of doped material.

3.7 I–V characteristics of the undoped and Co-doped Cu_2O films

The room temperature current–voltage (I–V) characteristics of undoped and Co-doped Cu_2O films. In this work, I–V characteristics are carried out using Ag as contact electrodes by applying voltage from +5 V to -5 V. The I–V curves are shown in Fig. 12. The linear I–V curves show an ohmic conducting nature of the films. When the

input voltage is positive, the I–V curves will be positive and when the input voltage is negative, the I–V curves will be negative. The linear curves show the high crystalline quality of the films.

4 Conclusion

In summary, all the films show the preferential orientation along (111) plane with good crystalline quality. The surface morphology of the films was investigated using FESEM. The spherical grains were gradually converted into cubic and needle-shaped structures when the doping level was raised (10 wt%). EDX analysis confirms the presence of Cu, O and Co in the Co doped Cu_2O films. HRTEM analyses revealed that the undoped and Co-doped Cu_2O films are predominantly exposed (111) crystal plane. The transmittance of the film decreases with increase in

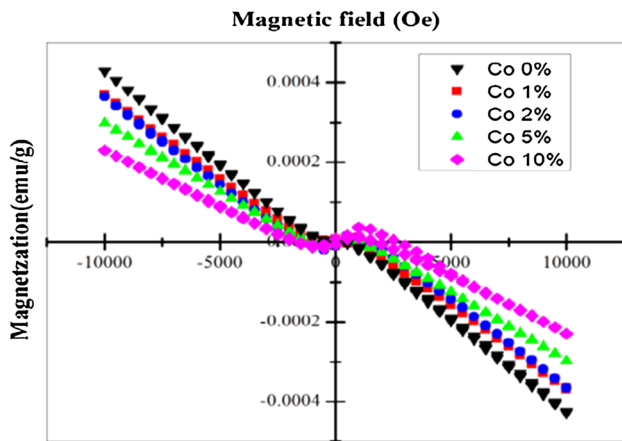


Fig. 11 Magnetic behavior of undoped and Co-doped Cu_2O films

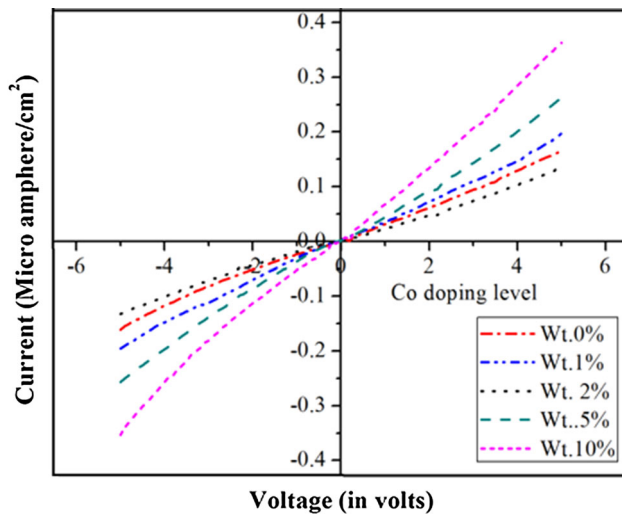


Fig. 12 Current versus voltage for undoped and Co-doped Cu_2O films

Co doping concentration. The magnetic properties (M–H) of the films were studied using VSM. The ferromagnetic (low magnetization field) properties are exhibited when the Co doping level is a maximum (10 wt%). The energy band gap value varies from 1.94 to 2.47 eV for Co doped Cu_2O . The electrical studies show the increase in current with the increase of Co doping level of the films. Such materials are fit for use in optoelectronic devices. Further investigations are needed to determine the magnetic and structural properties after annealing at suitable temperature.

Acknowledgements Our special thanks to Dr. R. Chandramohan, Principal, Sree Sevugan Annamalai College, Devakottai, Tamilnadu, India, for his kind encouragement. The Principal author A. T. Ravichandran thanks, UGC-MRP: F.No 41-937/2012(SR), New Delhi for the partial funding of the work through a major research Grant.

References

1. K. Mageshwari, R. Sathyamoorthy, *Mater. Sci. Semicond. Process.* **16**, 337 (2013)
2. S.L. Mammah, F.E. Opara, V.B. Omubo-Pepple, J.E.-E. Ntibi, S.C. Ezugwu, F.I. Ezema, *Nat. Sci.* **5**, 389 (2013)
3. L.-C. Chen, *Mater. Sci. Semicond. Process.* **16**, 1172 (2013)
4. L. Zhang, L. McMillon, J. McNatt, *Sol. Energy Mater. Sol. Cells* **108**, 230 (2013)
5. F. Bayansal, T. TasKoPru, B. Sahin, H.A. Cetinkara, *Miner. Met. Mater. Soc. ASM. Int.* (2014). doi:10.1007/s11661-014-2306-1
6. G. Fan, F. Li, *Chem. Eng. J.* **167**, 388 (2011)
7. H.S. Lim, D. Kwak, D.Y. Lee, K. Cho, *J. Am. Chem. Soc.* **129**, 4128 (2007)
8. P.A. Praveenjanantha, L.N.L. Perera, K.M.D.C. Jayathilaka, J.K.D.S. Jayanetti, D.P. Dissanayaka, W.P. Siripala, *Process. Tech. Sess.* **25**, 70 (2009)
9. V. Georgieva, M. Ristov, *Sol. Energy Mater. Sol. Cells* **73**, 67 (2002)
10. K. Han, M. Tao, *Sol. Energy Mater. Sol. Cells* **93**, 153 (2009)
11. X.P. Gao, J.L. Bao, G.L. Pan, H.Y. Zhu, P.X. Huang, F. Wu, D.Y. Song, *J. Phys. Chem. B* **108**, 5547 (2004)
12. J.M.D. Coey, M. Venkatesan, C.B. Fitzgerald, *Nat. Mater.* **4**, 173 (2005)
13. Y. Ghayeb, M.M. Momeni, A. Mozafari, *J. Mater. Sci. Mater. Electron.* (2016). doi:10.1007/s10854-016-5321-8
14. M.M. Momeni, *Indian J. Chem.* **55A**, 686 (2016)
15. M.M. Momeni, I. Ahadzadeh, *Mater. Res. Innov.* **20**, 44 (2016)
16. M.M. Momeni, Y. Ghayeb, Z. Ghonchehi, *Ceram. Int.* **41**, 8735 (2015)
17. M.M. Momeni, M. Mirhosseini, M. Chavoshi, A. Hakimizade, *J. Mater. Sci. Mater. Electron.* **27**, 3941 (2016)
18. M.M. Momeni, M. Hakimian, A. Kazempour, *Ceram. Int.* **41**, 13692 (2015)
19. S.N. Kale, S.B. Ogale, S.R. Shinde, M. Sahasrabudde, V. Kulkarni, R. Greene, T. Venkatesan, *Appl. Phys. Lett.* **82**, 2100 (2003)
20. M. Beekmana, J. Salvadorb, X. Shic, G.S. Nolasa, J. Yangb, *J. Alloys Compd.* **489**, 336 (2010)
21. P.E. de Jongh, D. Vanmaekelbergh, J.J. Kelly, *Chem. Commun.* **12**, 1069 (1999)
22. T.-L. Li, Y.-L. Lee, H. Teng, *J. Energy Environ. Sci.* **5**, 5315 (2012)
23. H.Y. Xu, C. Chen, L. Xu, J.K. Dong, *Thin Solid Films* **527**, 76 (2013)
24. M.M. Momeni, Y. Ghayeb, *Appl. Phys. A* **122**, 620 (2016)
25. M.M. Momeni, M. Hakimian, A. Kazempour, *Surf. Eng.* **32**, 514 (2016)
26. M.M. Momeni, Y. Ghayeb, M. Davarzadeh, *J. Alloys Compd.* **637**, 393 (2015)
27. M.M. Momeni, Y. Ghayeb, *J. Solid State Electrochem.* **20**, 683 (2016)
28. M.M. Momeni, Y. Ghayeb, *J. Mater. Sci. Mater. Electron.* **27**, 3318 (2016)
29. M.M. Momeni, *Mater. Res. Innov.* **20**, 317 (2016)
30. S.H. Jeong, E.S. Aydil, *J. Cryst. Growth* **311**, 4188 (2009)
31. X. Yu, X. Li, G. Zheng, Y. Wei, A. Zhang, B. Yao, *Appl. Surf. Sci.* **270**, 340 (2013)
32. M. Vila, C. Díaz-Guerra, J. Piqueras, *J. Phys. D Appl. Phys.* **43**, 135403 (2010). doi:10.1088/0022-3727/43/13/135403
33. Q. Zhang, W. Fan, L. Gao, *Appl. Catal. B* **76**, 168 (2007)
34. G.B. Dong, M. Zhang, W. Lan, P.M. Dong, X.P. Zhao, H. Yan, *J. Mater. Sci. Mater. Electron.* **20**, 193 (2009)
35. A.N. Banerjee, S. Nandy, C.K. Ghosh, K.K. Chattopadhyay, *Thin Solid Films* **515**, 7324 (2007)

36. M.M. Momeni, M. Mirhosseini, M. Chavoshi, *Ceram. Int.* **42**, 9133 (2016)
37. M.M. Momeni, Z. Nazari, *Ceram. Int.* **42**, 8691 (2016)
38. M. Abdel Rafea, N. Roushdy, *J. Phys. D: Appl. Phys.* **42**, 015413 (2008)
39. M.M. Momeni, A.A. Mozafari, *J. Mater. Sci. Mater. Electron.* (2016). doi:[10.1007/s10854-016-5163-4](https://doi.org/10.1007/s10854-016-5163-4)
40. M.M. Momeni, Y. Ghayeb, A.A. Mozafari, *J. Mater. Sci. Mater. Electron.* (2016). doi:[10.1007/s10854-016-5240-8](https://doi.org/10.1007/s10854-016-5240-8)
41. A. Vasuhi, R. John Xavier, R. Chandramohan, S. Muthkumaran, K. Dhanabalan, M. Ashokkumar, P. Parameswaren, *J. Mater. Sci. Mater. Electron.* **25**, 824 (2014)
42. S.M. Hosseinpour-Mashkani, M. Ramezani, A. Sobhani-Nasab, M. Esmaili-Zare, *J. Mater. Sci. Mater. Electron.* **26**, 6086 (2015)
43. S.M. Hosseinpour-Mashkani, M. Maddahfar, A. Sobhani-Nasab, *J. Electron. Mater.* **45**, 3612 (2016)
44. S.M. Hosseinpour-Mashkani, M. Maddahfar, A. Sobhani-Nasab, *J. Mater. Sci. Mater. Electron.* **27**, 474 (2016)
45. V. Senthamilselvi, K. Saravanakumar, R. Anandhi, A.T. Ravichandran, K. Ravichandran, *Optoelectron. Adv. Mater. Rapid Commun.* **5**, 1072 (2011)
46. P.-H. Hsieh, Y.-M. Lu, W.-S. Hwang, J.-J. Yeh, W.-L. Jang, *Surf. Coat. Technol.* **205**, S206 (2010)
47. M.M. Momeni, Y. Ghayeb, *J. Electroanal. Chem.* **751**, 43 (2015)
48. M.M. Momeni, Y. Ghayeb, *J. Appl. Electrochem.* **45**, 557 (2015)
49. M.M. Momeni, Y. Ghayeb, M. Davarzadeh, *J. Electroanal. Chem.* **739**, 149 (2015)
50. M.M. Momeni, *Appl. Surf. Sci.* **357**, 160 (2015)
51. S. Wang, H. Xu, L. Qian, X. Jia, J. Wang, Y. Liu, W. Tang, *J. Solid State Chem.* **182**, 1088 (2009)
52. N. Ekthammathat, T. Thongtem, S. Thongtem, *Appl. Surf. Sci.* **277**, 211 (2013)
53. R.P. Pal Singh, I.S. Hudiara, S. Panday, P. Kumar, S.B. Rana, *Int. J. Nanoelectron. Mater.* **9**, 1 (2016)
54. A.T. Ravichandran, K. Dhanabalan, K. Ravichandran, R. Mohan, K. Karthika, A. Vasuhi, B. Muralidharan, *Acta Metall. Sin. (Engl. Lett.)* **28**, 1041 (2015)
55. K. Maaz, A. Mumtaz, S.K. Hasanian, A. Ceylan, *J. Magn. Magn. Mater.* **308**, 289 (2007)
56. D.P. Joseph, T.P. David, S.P. Raja, C. Venkateswaran, *Mater. Charact.* **59**, 1137 (2008)
57. J. Antony, Y. Qiang, M. Faheem, D. Meyer, D.E. McCready, M.H. Engelhard, *Appl. Phys. Lett.* **90**, 013106 (2007)